

# Semiclassical Trajectory Perspective of Glory Rescattering in Strong-field Photoelectron Holography

L. G. Liao<sup>1,2</sup>, Q. Z. Xia<sup>3,\*</sup>, J. Cai<sup>4</sup>, and J. Liu<sup>2,5†</sup>

<sup>1</sup>*School of Physics, Peking University, Beijing 100871, China*

<sup>2</sup>*CAPT, HEDPS, and IFSA Collaborative Innovation Center of MoE, Peking University, Beijing 100871, China*

<sup>3</sup>*National Laboratory of Science and Technology on Computational Physics,*

*Institute of Applied Physics and Computational Mathematics, Beijing 100088, China*

<sup>4</sup>*School of Physics and Electronic Engineering, Jiangsu Normal University, Xuzhou 221116, China and*

<sup>5</sup>*Graduate School of China Academy of Engineering Physics, Beijing 100193, China*

We investigate theoretically the photoelectron momentum distribution (PMD) of the ionized atoms irradiated by a linearly polarized intense laser, focusing on the holography interference patterns in PMD that carry important information of the initial wavefunction of a tunneled electron and its experienced atomic potential in rescattering. With the help of Dyson series and semiclassical propagator, we calculate the scattering amplitudes in the cylindrical coordinate representation. In contrast to conventional recognitions that the photoelectron holography is the interference of two branches of electron trajectories, however, we find strikingly that infinite semiclassical trajectories can be deflected by the combined Coulomb potential and laser field into the same final momentum: The initial momenta are found to be distributed on a ring-shape curve in the transverse momentum plane and the initial positions of these trajectories are perpendicular to their initial momentum vectors. For the zero final transverse momentum, the above ring-source trajectories degenerate into the point-source axial caustic trajectories (or Glory trajectories) and the quantum interference of these trajectories will dramatically alter the scattering amplitudes that is termed as Glory rescattering effect. With following Berry's spirit of uniform approximation for Glory scattering in optics, we can finally derive a uniform formulation of the rescattering amplitude in the Bessel functions for the strong-field photoelectron holography (SFPH) patterns. Our results are in good agreement with solutions of the time-dependent Schrödinger equation and can account for recent photoelectron holography experiments. Important applications of our theory are also discussed.

## I. INTRODUCTION

Strong-field photoelectron holography (SFPH) provides a powerful tool for investigating the structure and dynamics of atoms and molecules [1–13]. The physics behind SFPH is that in analog to conventional optical holography, the modulation patterns in photoelectron momentum distribution (PMD) are the phase interference of diverse electron trajectories and therefore carry important informations of initial states of tunneled electrons and their experienced rescattering potentials [14–16]. Nevertheless, to correctly extract the information contained in the holographic patterns of PMDs, sophisticated nonperturbative theories for the photoionization and rescattering in combined Coulombic and intense laser fields are required.

Semiclassical dynamics can provide intuitive pictures for the strong field ionization and successfully explained the physical mechanisms behind many striking structures in PMD spectroscopy [17–21]. In the semiclassical description, the photoelectron experiences a tunneling through the electromagnetic field suppressed Coulomb barrier and then accelerated in the combined laser field and the Coulomb potential of its parent ion. The latter

process is termed as rescattering or recollision. SFPH is tightly related to the quantum interference in the rescattering process [22–26]. Numerically, PMDs can be obtained by directly integrating the time-dependent Schrödinger equation (TDSE) [3, 8, 27, 28] in full dimensionality (3D). Theoretically, quantum scattering theory based on strong field approximation (SFA) [29–31] as well as the Coulomb corrected strong field approximation (CCSFA) [32–34] has been successfully exploited to understand many interesting structures of PMDs. More recently, Gouy's phase [35] anomaly or Maslov phase [36] in strong field rescattering trajectories are addressed [37]. In the above discussions, two branches of trajectories, one is directly ionized trajectory, the other is rescattering trajectory, are considered. However, due to the existence of caustic singularity [38, 39], the scattering theories that coherently sum over two trajectories for each asymptotic momentum fail to analyze Glory effect, in which the contribution of infinite trajectories can dramatically modulate the scattering amplitude. In order to resolve this caustic singularity, the Glory rescattering theory (GRT) has been developed [40]. According to GRT, the infinite semiclassical trajectories are integrated to give rise to a pattern of Bessel function distribution. The results of GRT are also certificated by recent two-step model calculations [26]. Nevertheless, the GRT focuses on caustic singularity, i.e., the near-zero final transverse momentum region in PMDs. To extend the GRT to non-zero final transverse momentum region and give a uniform descrip-

\*xiaqinzhi@iapcm.ac.cn

†jliu@gscaep.ac.cn

tion to PMDs from the semiclassical trajectory perspective is urgently needed for practical SFPH applications.

On the other hand, M. V. Berry in 1960s has applied a uniform approximation theory to solve the Glory scattering problems in optics and developed a scattering amplitude formula that can be continually applied from small angle scattering to large angle or even the back scattering [41, 42]. Following the concept of the uniform approximation, in the present work, we extend the GRT by exploiting a semiclassical path integral to deduce a uniform formulation for all angles of forward and backward rescattering in PMDs. Our results are compared with TDSE calculations, the existing theories as well as the holography experiments.

The paper is organized as follows. In Sec. II, we present our theoretical formulation. Sec. III is our results and discussions.

Atomic units are used unless otherwise specified.

## II. THEORETICAL FORMULISM

### A. Scattering amplitude from the semiclassical trajectory perspective

We start with the Hamiltonian for atom-field interaction problem in the length gauge, which takes following form of  $H[\vec{r}(t), \vec{p}(t)] = \frac{p^2(t)}{2} + \vec{F}(t) \cdot \vec{r}(t) - \frac{1}{r(t)}$ . With exploiting the Dyson series [43] we have,  $U(t, 0) = U_0(t, 0) - i \int_0^t dt_0 U(t, t_0) V_L(t_0) U_0(t_0, 0)$ . Where  $U$  denotes the complete evolution operator in the combined Coulomb potential and laser field;  $U_0$  represents the evolution operators under pure Coulombic potential, and has the property of  $U_0(t_0, 0)|\psi(0)\rangle = |\psi(0)\rangle e^{iI_p t_0}$ , here  $I_p$  is the ionization potential and  $|\psi(0)\rangle$  denotes the initial wavefunction;  $V_L = \vec{F}(t) \cdot \vec{r}$  and  $\vec{F}(t)$  is the electric field.

With the help of Dyson's series, we thus have time dependent wavefunction  $|\psi(t)\rangle = U_0(t, 0)|\psi(0)\rangle - i \int_0^t dt_0 U(t, t_0) V_L(t_0) U_0(t_0, 0)|\psi(0)\rangle$ . The scattering amplitude of a continuum state with asymptotic momentum  $\vec{p}_f$  can be written as  $M_{\vec{p}_f} = \langle \vec{p}_f | \psi(t_f) \rangle = -i \int dt_0 \langle \vec{p}_f | U(t_f, t_0) V_L(t_0) U_0(t_0, 0) | \psi(0) \rangle$  with  $t_f \rightarrow \infty$ . With inserting an identity  $\int d\vec{p}_0 |\vec{p}_0\rangle \langle \vec{p}_0| \equiv 1$ , we have

$$M_{\vec{p}_f} = -i \iint dt_0 d\vec{p}_0 G(\vec{p}_f, t_f; \vec{p}_0, t_0) \mathcal{D}(\vec{p}_0, t_0) e^{iI_p t_0}. \quad (1)$$

Here  $\mathcal{D}(\vec{p}_0, t_0) = \langle \vec{p}_0 | V_L(t_0) | \psi(0) \rangle$  represents the dipole matrix element and the momentum-to-momentum propagator  $G(\vec{p}_f, t_f; \vec{p}_0, t_0) = \langle \vec{p}_f | U(t_f, t_0) | \vec{p}_0 \rangle$ .

In the semiclassical approximation [36, 44], the propagator  $G(\vec{p}_f, t_f; \vec{p}_0, t_0) = \mathcal{F}(\vec{p}_f, t_f; \vec{p}_0, t_0) e^{i\mathcal{S}(\vec{p}_f, t_f; \vec{p}_0, t_0)}$ , where the semiclassical phase  $\mathcal{S}(\vec{p}_f, t_f; \vec{p}_0, t_0) = \int_{t_0}^{t_f} dt (-\vec{r}(t) \cdot \dot{\vec{p}}(t) - H[\vec{r}(t), \vec{p}(t)])$ . We neglect the Maslov phase in holography patterns, and the reason is discussed in subsection C. The prefactor  $\mathcal{F} = [\frac{1}{(2\pi i)^3} \det(\frac{\partial^2 \mathcal{S}}{\partial p_0 \partial p_f})]^{1/2}$ .

Considering the case of linearized laser field that is polarized along  $z$  axis, the problem intrinsically has the rotational symmetry about the axial coordinate. We therefore introduce the cylindrical coordinate instead of Cartesian coordinate. Thus, Eq. (1) can be rewritten as

$$M_{\vec{p}_f} = \iiint dt_0 dp_{z0} dp_{\rho 0} d\phi p_{\rho 0} \mathcal{F} \cdot \mathcal{D} \cdot e^{i\mathcal{A}(\vec{p}_f, t_f; \vec{p}_0, t_0)} \quad (2)$$

Here,  $\mathcal{A} = \mathcal{S} + I_p t_0$ . Because  $\mathcal{F}$  and  $\mathcal{D}$  are slowly-varying functions, we treat Eq. (2) with the steepest descent method for the time integration as well as the momentum integrations. The saddle point condition for the time variable gives,

$$\frac{\partial \mathcal{A}}{\partial t_0} \Big|_{t_s} = 0. \quad (3)$$

With applying the steepest descent method to treat the integration on  $p_{z0}$  and  $p_{\rho 0}$ , we obtain the coordinates of the saddle points satisfying

$$z(t_s) = 0; \quad \vec{\rho}_s \cdot \vec{p}_{\rho s} = 0. \quad (4)$$

In the above deductions, we use the relation  $\frac{\partial \mathcal{A}}{\partial p_\rho} = x \cos \phi + y \sin \phi = \vec{\rho} \cdot \vec{p}_\rho / |\rho|$ . In contrast to conventional steepest descent method implemented in the Cartesian coordinates, in which the saddle point conditions give that the positions of the saddle points are located at origin, in our cylindrical coordinate representation, the saddle points might even not be on the symmetric  $z$ -axis. The second formula in Eq. (4) gives a constraint on the initial coordinates and momenta.

Then the scattering amplitude here becomes

$$M_{\vec{p}_f} \approx \int d\phi p_{\rho s} \left( \frac{(2\pi i)^3}{\det(\frac{\partial^2 \mathcal{A}}{\partial(t_0, p_{z0}, p_{\rho 0})})} \Big|_{t_s} \right)^{1/2} \mathcal{F}_s \mathcal{D}_s e^{i\mathcal{A}_s}. \quad (5)$$

where  $\mathcal{A}_s, \mathcal{F}_s$ , and  $\mathcal{D}_s$  represent the values at the saddle point  $(\vec{p}_s, t_s)$ ,

In the above integration, the phase  $\mathcal{A}_s$  is the implicit function of the azimuthal angle  $\phi$ . To treat this scattering amplitude integration, we closely follow the Berry's spirit of uniform approximation [41, 42] with renormalizing the angular variable. Let us introduce a new angular variable  $\varphi$ , which satisfies  $\phi = 0 \leftrightarrow \varphi = 0$ ,  $\phi = \pi \leftrightarrow \varphi = \pi$  and  $\mathcal{A}_s(\phi) = \bar{\mathcal{A}}_s(\varphi) \equiv \mathcal{A}_0 + \mathcal{A}_1 \cos(\varphi)$ , where  $\mathcal{A}_0 = (\mathcal{A}_s(\phi = 0) + \mathcal{A}_s(\phi = \pi))/2$  corresponds to the sum of the phases of the  $\phi = 0$  and  $\phi = \pi$  semiclassical photoelectron trajectories,  $\mathcal{A}_1 = (\mathcal{A}_s(\phi = 0) - \mathcal{A}_s(\phi = \pi))/2$  corresponds to the phase difference between the  $\phi = 0$  and  $\phi = \pi$  trajectories.

With the variable transformation, the scattering amplitude of Eq. (5) turns to be (see Appendix A for details),

$$M_{\vec{p}_f} \approx \int_0^{2\pi} d\varphi C(\varphi) e^{i(\mathcal{A}_0 + \mathcal{A}_1 \cos \varphi)}. \quad (6)$$

The prefactor  $C(\varphi)$  takes form,

$$C(\varphi) \propto \frac{\mathcal{D}_s}{\sqrt{\frac{d^2 \mathcal{A}_s}{dt_s^2}}} (\mathcal{A}_1 \cos \varphi)^{\frac{1}{2}} \frac{p_{\rho s}}{p_{\rho f}} \det \left( \frac{\partial(p_{zs}, p_{\rho s})}{\partial(p_{zf}, p_{\rho f})} \right). \quad (7)$$

We can approximate the the above function in the following form  $C(\varphi) \approx \frac{1}{2}(C(0) + C(\pi)) + \frac{1}{2}(C(0) - C(\pi)) \cos \varphi$ . Finally, the scattering amplitude integration can be evaluated by the Bessel functions in following explicit forms, that is termed as uniform Glory rescattering theory (UGRT).

$$\begin{aligned} & M_{\vec{p}_f} \\ & \approx \frac{1}{2} \int_0^{2\pi} d\varphi [(C(0) + C(\pi)) + (C(0) - C(\pi)) \cos \varphi] e^{i\mathcal{A}_1 \cos \varphi} \\ & = \frac{1}{2} (C(0) + C(\pi)) J_0(\mathcal{A}_1) - \frac{1}{2} i (C(0) - C(\pi)) J_1(\mathcal{A}_1) \end{aligned} \quad (8)$$

Let us now analyze the physics behind the above deductions. From the expression of Eq. (5), we see that for a given final photoelectron momentum, in contrast to conventional recognition of the two-trajectory interference, we find that infinite semiclassical trajectories can be deflected by the combined Coulomb potential and laser field into the same final momentum. This phenomenon is mentioned very recently only for the case of zero final transverse momentum [40], where the infinite trajectories of tunneling electrons at moment  $Re(t_s)$  on z-axis with equal transverse momentum are rescattered to the final states with zero transverse momentum, leading to so called caustic singularity [45]. Similar phenomenon is termed as the Glory scattering first discussed in optics and then extended to particle scattering by Wheeler [39, 46, 47]. The quantum interference of the infinite Glory trajectories will manipulate the scattering amplitude with showing a bright fringe around the zero angle in SFPH. This picture is apparent and can be readily imagined by considering the cylindrical symmetry of the geometric configuration of the problem.

Our above deductions explicitly indicate that the infinite-trajectory interference can emerge also for nonzero final transverse momenta. According to Eq. (4) and from our detailed calculations of these semiclassical trajectories (see Fig. 1 and 2 in following section), we find that the initial position of these trajectories are no longer on the symmetric z-axis and found to be distributed on a ring-shape curve in the transverse coordinate plane. The initial transverse momentum are perpendicular to the initial position vectors according the constraint of Eq. (4).

Moreover, the expression of Eq. (8) shows that the scattering amplitude can be expressed in the sum of zeroth-order and first-order Bessel functions in uniform approximation. The variable  $\mathcal{A}_1$  in the Bessel functions represents the phase difference of two distinct semiclassical trajectories corresponding to  $\phi = 0$  and  $\phi = \pi$ , respectively. When the final transverse momentum tends to 0,  $C(0)$  equals to  $C(\pi)$ , and Eq. (8) will reduce to the

formulation of GRT in Ref. [40]. In GRT,  $M_{\vec{p}}$  can be written in the following form  $|M_{\vec{p}}|^2 \sim \varpi p_{\perp g} b_g J_0^2(p_{\perp} b_g)$  in which  $p_{\perp g}$  is the initial transverse momentum of the Glory trajectory at the tunneling exit,  $b_g$  is the emergent impact parameter of the Glory trajectory, and  $\varpi$  is the weight of the Glory trajectory. In this situation, we note that the phase difference of  $\mathcal{A}_1$  in Eq. (8) approximately equals to  $p_{\perp} b_g$ , here  $p_{\perp}$  is the final transverse momentum.

## B. Calculations of semiclassical trajectories and associated phase accumulations

States at some typical times that an electron experiences in its ionization process are listed in TABLE I, in which  $Re(t_s)$  is the real part of saddle point time  $t_s$ . The condition of saddle point according to Eq. (3) is obtained by solving saddle point equation within the strong-field approximation (see, e.g., [48, 49])  $\frac{1}{2}(\tilde{p}_{\rho s}^2 + [\tilde{p}_{zs} + A(t_s)]^2) + I_p = 0$ , here  $\tilde{p}$  is the canonical momentum. The corresponding kinetic momenta at saddle point are then given by  $p_{zs} = \tilde{p}_{zs} + A(t_s)$  and  $p_{\rho s} = \tilde{p}_{\rho s}$ .

Under the constraint of saddle point condition of Eq. (4), for a given final momentum, we can use shooting method [50] to obtain the initial conditions of semiclassical trajectories, by solving following Newton equations of motion numerically using the Runge-Kutta-Fehlberg method,  $\dot{\vec{p}} = -\vec{F}(t) - \vec{\nabla}V(\vec{r}(t))$  where  $V(\vec{r}(t))$  is the atomic potential. The asymptotic condition is that  $t \rightarrow \infty$ ,  $\vec{p} \rightarrow \vec{p}_f$ . In semiclassical treatment, the phase of each trajectory is divided into two parts: ionization process phase and acceleration process phase. The phase accumulated during ionization process is given by  $\mathcal{A}(t_s \rightarrow Re(t_s)) = -\frac{1}{2} \int_{t_s}^{Re(t_s)} (\tilde{p}_{\rho s}^2 + [\tilde{p}_{zs} + A(t)]^2) dt$ . The phase accumulated during the acceleration process can be expressed as  $\mathcal{A}(t_f; Re(t_s)) = -\int_{Re(t_s)}^{t_f} dt \{ \dot{\vec{p}}(t) \cdot \vec{r}(t) + H[\vec{r}(t), \vec{p}(t)] \}$  [51].

With these semiclassical trajectories and corresponding phases, we can reconstruct the photoelectron momentum spectrum according to Eq. (8).

## C. Some remarks

In conventional treatments, one directly treat integral of Eq. (1) with steepest descent method for all momentum variables in Cartesian coordinates, the initial positions of tunneled electron will locate on z-axis. Then,

TABLE I: States of an electron in ionization process

Time	State description	Position and/or momentum
$t_s$	saddle point	$z_s = 0, \vec{p}_s \cdot \vec{p}_{\rho s} = 0, \vec{p}_{zs}, \vec{p}_{\rho s}$
$Re(t_s)$	tunneling exit	$\vec{r}_0 = Re \int_{t_s}^{Re(t_s)} (\vec{p} + A(t)) dt, \vec{p}_s$
$t_f = \infty$	final state	$\vec{p}_f, \dot{\vec{p}} = -\vec{F}(t) - \vec{\nabla}V(\vec{r}(t))$

within half a laser cycle there are usually two trajectories (one is directly ionized trajectory, the other is rescattering trajectory) can reach the same final momentum. The two-trajectory interference is used to explain for the SFPH where the modulation fringe can be expressed in the cosine function of the phase difference between the two trajectories. Recently, the Gouy's phase [35] is introduced to the two-trajectory strong-field interference picture in a 3D model to compensate for the divergence of the preexponential factors of the semiclassical propagator at focal points [37]. As a result, phase difference in the cosine function will be modified by a  $\nu\pi/2$  phase, where  $\nu$  is the Maslov index [52–55]. In fact, due to the cylindrical symmetry of the problem, infinite ring-source trajectories can converge to the same final momentum state, the quantum interference of the ring-source trajectories will give rise to the pattern in PMDs of Bessel functions instead of cosine functions. Within the framework of UGRT, the Maslov phases of different trajectories vanish. This is because in the representation of cylindrical coordinates, due to the cylindrical symmetry, the system essentially reduce to a 2D problem under the uniform approximation, in which the preexponential factors of the semiclassical propagator keep finite along the rescattering trajectories (i.e., no focal points) according to our detailed calculations.

### III. APPLICATIONS

#### A. Hydrogen atom in linearly laser fields

As a demonstration, we consider a hydrogen atom irradiated by a few-cycle linearly polarized infrared laser pulse. The vector potential of laser field is

$$A = -\frac{A_0}{\omega} \sin^2\left(\frac{\pi t}{t_p}\right) \sin(\omega t) \vec{e}_z. \quad (9)$$

The laser field is present between  $t = 0$  and  $t = t_p$  and  $\vec{e}_z$  is the unit vector pointing in polarization direction. The electric field is obtained by  $\vec{F} = -\frac{1}{c} \frac{\partial A}{\partial(t)}$ .

##### 1. Ring-source semiclassical trajectories

We use shooting method to obtain semiclassical trajectories for a given final momentum under the constraint of saddle point conditions given by Eq. (4). Our numerical results show that there are infinite semiclassical trajectories deflected by the combined Coulomb potential and laser field into the same final momentum. In Fig. 1 (a) and (b), we draw some typical trajectories of the tunneling electron in coordinate space as well as momentum space, and all of these trajectories reach the same final momentum of  $p_{zf} = 0.66$ ,  $p_{xf} = 0.12$  and  $p_{yf} = 0$  when  $t_f \rightarrow \infty$ . From Fig. 1 (c, d), we see interestingly that the initial momenta of these semiclassical trajectories are

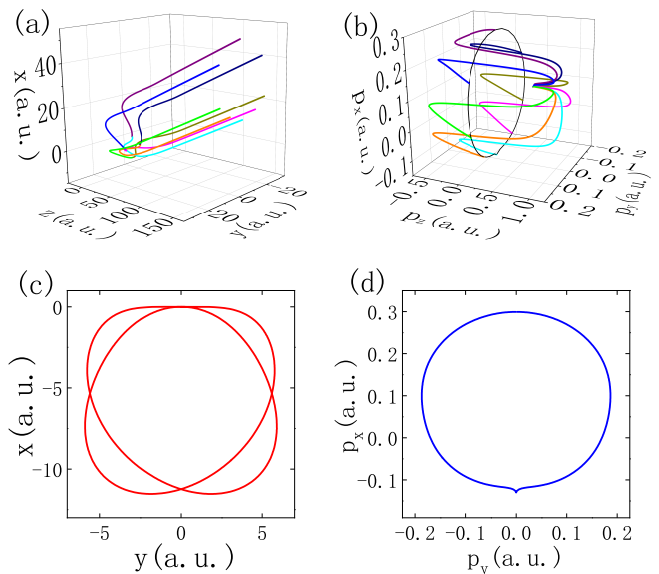


FIG. 1: Photoelectron semiclassical trajectories in coordinate space (a) and momentum space (b) for the final state of  $p_{zf} = 0.66a.u.$ ,  $p_{xf} = 0.12a.u.$ ,  $p_{yf} = 0$ . The initial positions on the projected x-y plane (c) and initial transverse momenta on the projected  $p_x$ - $p_y$  plane (d). The laser parameters are  $\lambda = 1200nm$  and  $I = 8.7 \times 10^{13}W/cm^2$ .

distributed in a ring, and the initial coordinates are no longer on the z axis and show a symmetric double-ring structure. After the acceleration of the laser field and the scattering of the nuclear Coulomb potential, these photoelectrons are finally scattered into the same final momentum (see Fig. 1 (b)).

Fig. 2 (a) and (b) shows the initial transverse momentum  $p_{\rho 0}$ , position  $\rho_0$  and azimuthal angle  $\phi_0$  with respect to final transverse momentum  $p_{xf}$  for the fixed final momentum  $p_{zf}=0.6$ ,  $p_{yf}=0$ . When final transverse momenta  $p_{xf}$  tends to 0, the initial transverse momentum becomes independent on  $\phi_0$ , and the initial positions  $\rho_0$  tends to zero. This corresponds to Glory rescattering trajectory as shown in Fig. 2 (c). For small  $p_{xf}$  of 0.03, in Fig. 2 (d), we also draw the joint distribution of the initial positions and initial momenta of photoelectron trajectories, which forms ring source similar to that of Fig. 1.

Interestingly, with increasing the transverse final momentum more ( $> 0.16$ ), our calculations show some classical trajectory forbidden regions denoted by the black areas in Fig. 2 (a) and (b). For instance, we plot, for the case of  $p_{xf} = 0.2$ , the initial transverse momenta of photoelectron trajectories in Fig. 2 (e) and the initial positions on the projected x-y plane Fig. 2 (f). In our calculations, we confine our initial positions of tunneling electrons within 16 a.u. distance to z-axis. To apply our UGRT to these situations, we need to make the analytical extension of the solutions to the forbidden regions, as indicated by the dashed lines in Fig. 2 (e) and (f).

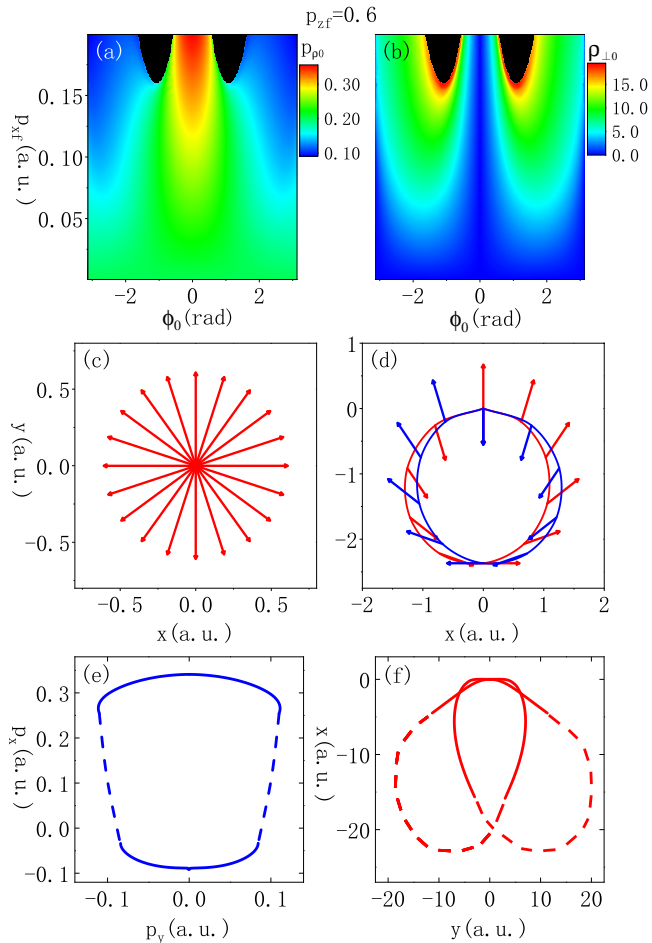


FIG. 2: For  $p_{zf} = 0.6$  a.u.,  $p_{yf} = 0$  a.u. and  $p_{xf}$  varied from 0 to 0.2 a.u., we present the calculated initial transverse momentum of  $p_{\rho 0}$  depending on azimuthal angle of  $\phi_0$  (a), and initial displacement of  $\rho_0$  to z-axis depending on azimuthal angle of  $\phi_0$  (b). In (c), for  $p_{xf}=0$  corresponding to the Glory caustic singularity, the initial positions are exactly at origin on the projected x-y plane, the initial transverse momenta are schematically by red arrows. In (d), for nonzero final transverse momentum of  $p_{xf} = 0.03$  a.u., we plot the initial positions on the projected x-y plane and the initial transverse momenta schematically by red arrows. The initial transverse momenta of photoelectron trajectories when  $p_{xf} = 0.2$  a.u. (e) and the corresponding initial positions on the projected x-y plane (f). The black areas in (a) and (b) represent the classical trajectory forbidden regions. The dashed lines in (e) and (f) is the analytical extension of the solutions to the forbidden regions. The laser parameters are  $\lambda = 1200\text{nm}$  and  $I = 8.7 \times 10^{13}\text{W/cm}^2$ .

## 2. Calculations of PMDs

To validate our theory, we also solve the time-dependent Schrödinger equation (TDSE) of a hydrogen (H) atom in infrared few-cycle linearly polarized laser field with a generalized pseudo-spectral method [56]. The

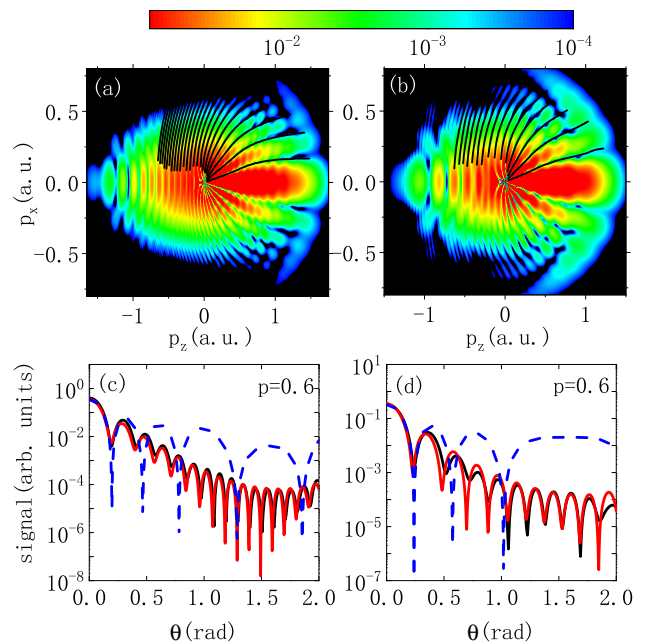


FIG. 3: In panels of (a) and (b), we show the PMDs for the hydrogen ionized by laser pulses with  $8.7 \times 10^{13}\text{W/cm}^2$  intensity calculated by TDSE, and the interference fringes predicted by our UGRT (black lines). In panels of (c) and (d), we plot the momentum distributions corresponding to fixed final momenta  $p=0.6$ . from calculations of TDSE (black lines), UGRT (red lines), and GRT (blue dash), respectively. The wavelength of laser pulses are  $\lambda = 1600\text{nm}$  [(a), (c)] and  $\lambda = 1200\text{nm}$  [(b), (d)]. In (c) and (d), scattering angle  $\theta = \arctan(\frac{p_{\rho f}}{p_{zf}}$ .

corresponding Hamiltonian is  $H[\vec{r}(t), \vec{p}(t)] = \frac{p^2(t)}{2} + \vec{F}(t) \cdot \vec{r}(t) - \frac{1}{r(t)}$ .

In Fig. 3, we compare our theoretical results with TDSE for varied laser wavelengths. From Fig. 3 (a) and (b) we can clearly see that the fringes calculated using UGRT is highly consistent with the results of TDSE. UGRT can precisely predict the positions of interference fringes even for the large scattering angles. The 1D slices of PMDs at the fixed final momenta  $p$  in Fig. 3 (c) and (d) show that the results of UGRT can also quantitatively predict the scattering amplitudes. As a comparison, the GRT can only give a good prediction inside the first scattering minimum but fails to predict both fringe positions and scattering amplitudes for the higher-order fringes.

For the small scattering angle, the scattering amplitude predicted by the two-trajectory interference models (even with Gouy's phase modification) diverges because prefactor  $\det(\frac{\partial \vec{p}_s}{\partial \vec{p}_f})$  there tends to infinite [37]. In our UGRT and GRT, the presence of the term of the square root of the phase difference in the prefactor (see Eq. (7)) will eliminate this singularity. When the final transverse momentum is large, i.e., for the large scattering angles, the phase differences increase. The Bessel functions then reduce to the simple cosine functions in the asymptotical

TABLE II: Optical analogs of SFPH theories ( $\Delta S$  denotes the phase difference of semiclassical trajectories)

Theory	Interference picture	Interference formula	Optical analogs
conventional models	two-trajectory interference	$\cos(\Delta S)$	double slit interference
UGRT	ring-source infinite trajectories	$C_0 J_0(\Delta S) + C_1 J_1(\Delta S)$	ring-source diffraction
GRT	point-source infinite trajectories	$J_0(\Delta S)$	point-source diffraction

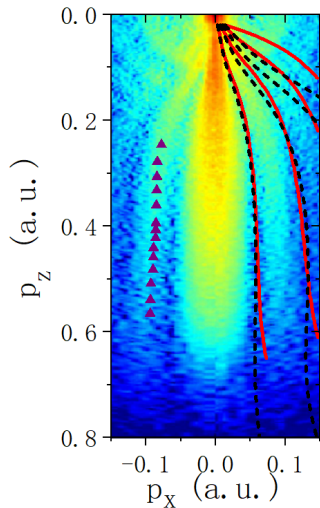


FIG. 4: Experimental holographic pattern and positions of the dark fringes calculated by UGRT (red lines), GRT (black dash) and CCSFA (purple triangles). The experimental data is extracted from Ref [8], where the metastable (6s) Xe atoms with ionization potential 0.14 a.u. are ionized with linearly polarized mid-infrared laser. The laser parameters are  $\lambda = 7\mu m$  and  $I = 7.1 \times 10^{11} W/cm^2$ .

forms of  $J_\alpha(x) \rightarrow \sqrt{\frac{2}{\pi x}} \cos(x - \frac{\alpha\pi}{2} - \frac{\pi}{4})$ ,  $\alpha$  is the order of the Bessel function.

### B. Application to experiment of Xeon

We now apply our theory to the experiment of Xeon (the red lines in Fig. 4). The experiments of metastable (6s) Xe atoms in this figure is using 7000 nm laser field [8]. As a comparison, we also plot the results predicted by other theories such as GRT (black dash) and CCSFA (purple solid triangles). According to CCSFA, the coherent summation of the two paths leads to  $\cos \Delta S$ -type oscillations in holography patterns. We can see that CCSFA even fails to predict the position of the first dark fringe, while GRT and UGRT are in perfect agreement with the experiment in this region. However, the discrepancy between the GRT and UGRT becomes more apparent for the third or higher order fringes. We hope that these theoretical predictions can be calibrated in future by SFPH experiments with higher resolution.

## IV. CONCLUSIONS

We investigate the PMDs of the ionized atoms irradiated by a linearly polarized strong laser field and provide a semiclassical trajectory perspective of Glory rescattering in SFPH. We calculate the scattering amplitudes in the cylindrical coordinate representation and finally derive a uniform formulation in the Bessel functions for the SFPH patterns. Our results are also in good agreement with solutions of the TDSE calculations and can give explanations to recent photoelectron holography experiments of Xe atoms. Compared with existing theories (see Table II), our UGRT provides a distinct ring-source infinite-trajectory interference description for photoelectron holograph patterns analogous to ring-source diffraction in optics. Our results of uniform approximation can also be applied to molecule and nondipole situations, related works are undergoing. Our work therefore have important implications in both theoretical aspects and the practical applications of SFPH.

## ACKNOWLEDGMENTS

This work is supported by the National Natural Science Foundation of China (Grants No. 11775030 and No. 11974057) and NSAF (Grant No. U1930403).

### Appendix A: Uniform approximation

From Eq. (5) we can see that the phase  $\mathcal{A}_s$  is the implicit function of the azimuthal angle  $\phi$ . To treat this scattering amplitude integration, we closely follow the Berry's spirit of uniform approximation [41, 42] with renormalizing the angular variable. Let us introduce a new angular variable  $\varphi$ , which satisfies  $\phi = 0 \leftrightarrow \varphi = 0$ ,  $\phi = \pi \leftrightarrow \varphi = \pi$  and  $\mathcal{A}_s(\phi) = \bar{\mathcal{A}}_s(\varphi) \equiv \mathcal{A}_0 + \mathcal{A}_1 \cos(\varphi)$ . Where  $\mathcal{A}_0 = (\mathcal{A}_s(\phi = 0) + \mathcal{A}_s(\phi = \pi))/2$  corresponds to the sum of the phases of the  $\phi = 0$  and  $\phi = \pi$  semiclassical photoelectron trajectories,  $\mathcal{A}_1 = (\mathcal{A}_s(\phi = 0) - \mathcal{A}_s(\phi = \pi))/2$  corresponds to the phase difference between the  $\phi = 0$  and  $\phi = \pi$  trajectories. Further, we can get

$$\frac{d\phi}{d\varphi} = \frac{d\bar{\mathcal{A}}_s}{d\varphi} / \frac{d\mathcal{A}_s}{d\phi} = \frac{\mathcal{A}_1 \sin\varphi}{L_\phi}. \quad (\text{A1})$$

Where  $L_\phi = -\frac{d\mathcal{A}}{d\phi}$  is the photoelectron angular momentum along the polarization direction. For linearly polarized laser field, the mirror symmetry will lead to  $\frac{d\mathcal{A}_s}{d\phi} = 0$

at  $\phi = 0$  and  $\pi$ . Both the denominator and numerator in Eq. (A1) become zeros when  $\phi = 0$  and  $\pi$ . With using L'Hospital's rule, we have

$$\frac{d\phi}{d\varphi} = \frac{d(\mathcal{A}_1 \sin\varphi)/d\phi}{dL_\phi/d\phi} = \frac{d(\mathcal{A}_1 \sin\varphi)/d\varphi}{dL_\phi/d\phi} / \left(\frac{d\phi}{d\varphi}\right). \quad (\text{A2})$$

$$\frac{d\phi}{d\varphi} = (\mathcal{A}_1 \cos\varphi / \frac{dL_\phi}{d\phi})^{\frac{1}{2}}. \quad (\text{A3})$$

With the variable transformation, the scattering amplitude of Eq. (5) turns to be

$$M_{\vec{p}_f} \approx \int_0^{2\pi} d\varphi C(\varphi) e^{i(\mathcal{A}_0 + \mathcal{A}_1 \cos\varphi)}. \quad (\text{A4})$$

Where  $C(\varphi)$  is the prefactor in the scattering amplitude integral which takes the following form

$$C(\varphi) = e^{i\mathcal{A}_0} \mathcal{F}_s \mathcal{D}_s p_{\rho_s} \left(\frac{\partial^2 \mathcal{A}_s}{\partial t_s^2}\right)^{-\frac{1}{2}} \left(\frac{(2\pi i)^3 \mathcal{A}_1 \cos\varphi}{\frac{dL_\phi}{d\phi} \det\left(\frac{\partial^2 \mathcal{A}_s}{\partial(p_{zs}, p_{\rho_s})}\right)}\right)^{\frac{1}{2}}. \quad (\text{A5})$$

$\frac{dL_\phi}{d\phi} = -\frac{d^2 \mathcal{A}_s}{d\phi_0^2}$ . When  $\varphi = 0$  and  $\varphi = \pi$ , we can prove the property that (proved in Appendix B)

$$\frac{d^2 \mathcal{A}_s}{d\phi_0^2} \det \frac{\partial^2 \mathcal{A}_s}{\partial(p_{\rho_s}, p_{zs})} = \det \left(\frac{\partial^2 \mathcal{A}_s}{\partial(p_{zs}, p_{\rho_s}, \phi_0)}\right). \quad (\text{A6})$$

Furthermore,

$$p_{\rho_s}^2 / \det \left(\frac{\partial^2 \mathcal{A}_s}{\partial(p_{zs}, p_{\rho_s}, \phi_0)}\right) = \left(\det \left(\frac{\partial^2 \mathcal{A}_s}{\partial \vec{p}_s^2}\right)\right)^{-1} \quad (\text{A7})$$

In semiclassical model, the prefactor  $\mathcal{F}_s \propto \left(\det \left(\frac{\partial^2 \mathcal{A}_s}{\partial \vec{p}_s \partial \vec{p}_f}\right)\right)^{\frac{1}{2}}$ . We can combine the two determinants in Eq. (A5),  $\det \left(\frac{\partial^2 \mathcal{A}_s}{\partial \vec{p}_s \partial \vec{p}_f}\right)^{\frac{1}{2}} \left(\det \left(\frac{\partial^2 \mathcal{A}_s}{\partial \vec{p}_s^2}\right)\right)^{-1} = \det \left(\frac{\partial \vec{p}_z}{\partial \vec{p}_f}\right)$ .

Under the cylindrical symmetry of linearly polarized fields, we have

$$\det \left(\frac{\partial \vec{p}_s}{\partial \vec{p}_f}\right) = \frac{p_{\rho_s}}{p_{\rho_f}} \det \left(\frac{\partial(p_{zs}, p_{\rho_s})}{\partial(p_{zf}, p_{\rho_f})}\right) \quad (\text{A8})$$

Substitute Eq. (A8) into Eq. (A5), we get the prefactor of following form,

$$C(\varphi) \propto \frac{\mathcal{D}_s}{\sqrt{\frac{d^2 \mathcal{A}_s}{dt_s^2}}} (\mathcal{A}_1 \cos\varphi)^{\frac{1}{2}} \frac{p_{\rho_s}}{p_{\rho_f}} \det \left(\frac{\partial(p_{zs}, p_{\rho_s})}{\partial(p_{zf}, p_{\rho_f})}\right). \quad (\text{A9})$$

Based on the above derivation, we can approximate the scattering amplitude integral in cylindrical coordinates

to the form expressed by Bessel functions, and finally get the Eq. (8).

## Appendix B

Under the saddle point condition of our derivation,

$$\frac{\partial \mathcal{A}_s}{\partial p_{z0}} = 0 \quad \frac{\partial \mathcal{A}_s}{\partial p_{\rho0}} = 0 \quad (\text{B1})$$

Differentiating the above equation,

$$\begin{aligned} d\left(\frac{\partial \mathcal{A}_s}{\partial p_{z0}}\right) &= \frac{\partial^2 \mathcal{A}_s}{\partial p_{z0}^2} dp_{z0} + \frac{\partial^2 \mathcal{A}_s}{\partial p_{z0} \partial p_{\rho0}} dp_{\rho0} + \frac{\partial^2 \mathcal{A}_s}{\partial p_{z0} \partial \phi_0} d\phi_0 = 0 \\ d\left(\frac{\partial \mathcal{A}_s}{\partial p_{\rho0}}\right) &= \frac{\partial^2 \mathcal{A}_s}{\partial p_{\rho0}^2} dp_{\rho0} + \frac{\partial^2 \mathcal{A}_s}{\partial p_{z0} \partial p_{\rho0}} dp_{z0} + \frac{\partial^2 \mathcal{A}_s}{\partial p_{\rho0} \partial \phi_0} d\phi_0 = 0. \end{aligned} \quad (\text{B2})$$

According to the total differential formula, we have the following properties,

$$\begin{aligned} d^2 \mathcal{A}_s &= \frac{\partial^2 \mathcal{A}_s}{\partial p_{z0}^2} dp_{z0}^2 + \frac{\partial^2 \mathcal{A}_s}{\partial p_{\rho0}^2} dp_{\rho0}^2 + \frac{\partial^2 \mathcal{A}_s}{\partial \phi_0^2} d\phi_0^2 \\ &+ 2 \frac{\partial^2 \mathcal{A}_s}{\partial p_{z0} \partial p_{\rho0}} dp_{z0} dp_{\rho0} + 2 \frac{\partial^2 \mathcal{A}_s}{\partial p_{\rho0} \partial \phi_0} dp_{\rho0} d\phi_0 + 2 \frac{\partial^2 \mathcal{A}_s}{\partial \phi_0 \partial p_{z0}} d\phi_0 dp_{z0} \end{aligned} \quad (\text{B3})$$

Use the above properties we can get the property we need in Appendix A.

$$\begin{aligned} \det \left(\frac{\partial^2 \mathcal{A}_s}{\partial(p_{z0}, p_{\rho0})}\right) \frac{d^2 \mathcal{A}_s}{d\phi_0^2} &= \left(\frac{\partial^2 \mathcal{A}_s}{\partial p_{z0}^2} \frac{\partial^2 \mathcal{A}_s}{\partial p_{\rho0}^2} - \left(\frac{\partial^2 \mathcal{A}_s}{\partial p_{z0} \partial p_{\rho0}}\right)^2\right) \\ &\cdot \left(\frac{\partial^2 \mathcal{A}_s}{\partial \phi_0^2} + \frac{\partial^2 \mathcal{A}_s}{\partial p_{\rho0} \partial \phi_0} \frac{dp_{\rho0}}{d\phi_0} + \frac{\partial^2 \mathcal{A}_s}{\partial \phi_0 \partial p_{z0}} \frac{dp_{z0}}{d\phi_0}\right) \\ &= \frac{\partial^2 \mathcal{A}_s}{\partial p_{z0}^2} \frac{\partial^2 \mathcal{A}_s}{\partial p_{\rho0}^2} \frac{\partial^2 \mathcal{A}_s}{\partial \phi_0^2} - \left(\frac{\partial^2 \mathcal{A}_s}{\partial p_{z0} \partial p_{\rho0}}\right)^2 \frac{\partial^2 \mathcal{A}_s}{\partial \phi_0^2} \\ &- \left(\frac{\partial^2 \mathcal{A}_s}{\partial p_{z0} \partial \phi_0}\right)^2 \frac{\partial^2 \mathcal{A}_s}{\partial p_{\rho0}^2} - \left(\frac{\partial^2 \mathcal{A}_s}{\partial p_{\rho0} \partial \phi_0}\right)^2 \frac{\partial^2 \mathcal{A}_s}{\partial p_{z0}^2} \\ &+ 2 \frac{\partial^2 \mathcal{A}_s}{\partial p_{\rho0} \partial \phi_0} \frac{\partial^2 \mathcal{A}_s}{\partial p_{z0} \partial p_{\rho0}} \frac{\partial^2 \mathcal{A}_s}{\partial p_{z0} \partial \phi_0} \\ &= \det \left(\frac{\partial^2 \mathcal{A}_s}{\partial(p_{z0}, p_{\rho0}, \phi_0)}\right). \end{aligned} \quad (\text{B4})$$

[1] F. Lindner, M. G. Schätzel, H. Walther, A. Baltuška, E. Goulielmakis, F. Krausz, D. B. Milošević, D. Bauer, W. Becker, and G. G. Paulus, Attosecond Double-Slit Experiment, *Phys. Rev. Lett.* **95**, 040401 (2005).

[2] R. Gopal, K. Simeonidis, R. Moshhammer, T. Ergler, M. Dürr, M. Kurka, K.-U. Kühnel, S. Tschuch, C.-D. Schröter, D. Bauer, J. Ullrich, A. Rudenko, O. Herrwerth, T. Uphues, M. Schultze, E. Goulielmakis, M. Uib-

- eracker, M. Lezius, and M. F. Kling, Three-Dimensional Momentum Imaging of Electron Wave Packet Interference in Few-Cycle Laser Pulses, *Phys. Rev. Lett.* **103**, 053001 (2009).
- [3] Y. Huismans, A. Rouzée, A. Gijsbertsen, J. Jungmann, A. Smolkowska, P. Logman, F. Lepine, C. Cauchy, S. Zamith, T. Marchenko, et al., Time-resolved holography with photoelectrons, *Science* **331**, 61 (2011).
- [4] X.-B. Bian, Y. Huismans, O. Smirnova, K.-J. Yuan, M. Vrakking, and A. D. Bandrauk, Subcycle interference dynamics of time-resolved photoelectron holography with midinfrared laser pulses, *Phys. Rev. A* **84**, 043420 (2011).
- [5] P. A. Korneev, S. V. Popruzhenko, S. P. Goreslavski, T.-M. Yan, D. Bauer, W. Becker, M. Kübel, M. F. Kling, C. Rödel, M. Wünsche, and G. G. Paulus, Interference Carpets in Above-Threshold Ionization: From the Coulomb-Free to the Coulomb-Dominated Regime, *Phys. Rev. Lett.* **108**, 223601 (2012).
- [6] X. Xie, S. Roither, D. Kartashov, E. Persson, D. G. Arbó, L. Zhang, S. Gräfe, M. S. Schöffler, J. Burgdörfer, A. Baltuška, and M. Kitzler, Attosecond Probe of Valence-Electron Wave Packets by Subcycle Sculpted Laser Fields, *Phys. Rev. Lett.* **108**, 193004 (2012).
- [7] X.-B. Bian and A. D. Bandrauk, Attosecond time-resolved imaging of molecular structure by photoelectron holography, *Phys. Rev. Lett.* **108**, 263003 (2012).
- [8] Y. Huismans, A. Gijsbertsen, A. S. Smolkowska, J. H. Jungmann, A. Rouzée, P. S. W. M. Logman, F. Lépine, C. Cauchy, S. Zamith, T. Marchenko, J. M. Bakker, G. Berden, B. Redlich, A. F. G. van der Meer, M. Y. Ivanov, T.-M. Yan, D. Bauer, O. Smirnova, and M. J. J. Vrakking, Scaling Laws for Photoelectron Holography in the Midinfrared Wavelength Regime, *Phys. Rev. Lett.* **109**, 013002 (2012).
- [9] D. D. Hickstein, P. Ranitovic, S. Witte, X.-M. Tong, Y. Huismans, P. Arpin, X. Zhou, K. E. Keister, C. W. Hogle, B. Zhang, C. Ding, P. Johnsson, N. Tushima, M. J. J. Vrakking, M. M. Murnane, and H. C. Kapteyn, Direct Visualization of Laser-Driven Electron Multiple Scattering and Tunneling Distance in Strong-Field Ionization, *Phys. Rev. Lett.* **109**, 073004 (2012).
- [10] M. Meckel, A. Staudte, S. Patchkovskii, D. Villeneuve, P. Corkum, R. Dörner, and M. Spanner, Signatures of the continuum electron phase in molecular strong-field photoelectron holography, *Nature Physics* **10**, 594 (2014).
- [11] M. Haertelt, X.-B. Bian, M. Spanner, A. Staudte, and P. B. Corkum, Probing molecular dynamics by laser-induced backscattering holography, *Phys. Rev. Lett.* **116**, 133001 (2016).
- [12] S. G. Walt, N. B. Ram, M. Atala, N. I. Shvetsov-Shilovski, A. Von Conta, D. Baykusheva, M. Lein, and H. J. Wörner, Dynamics of valence-shell electrons and nuclei probed by strong-field holography and rescattering, *Nature communications* **8**, 1 (2017).
- [13] N. Werby, A. S. Maxwell, R. Forbes, P. H. Bucksbaum, and C. F. d. M. Faria, Dissecting subcycle interference in photoelectron holography, *Phys. Rev. A* **104**, 013109 (2021).
- [14] P. B. Corkum and F. Krausz, Attosecond science, *Nature physics* **3**, 381 (2007).
- [15] P. B. Corkum, Recollision physics, *Phys. Today* **64**, 36 (2011).
- [16] H. Kang, A. S. Maxwell, D. Trabert, X. Lai, S. Eckart, M. Kunitski, M. Schöffler, T. Jahnke, X. Bian, R. Dörner, and C. F. d. M. Faria, Holographic detection of parity in atomic and molecular orbitals, *Phys. Rev. A* **102**, 013109 (2020).
- [17] P. B. Corkum, N. H. Burnett, and F. Brunel, Above-threshold ionization in the long-wavelength limit, *Phys. Rev. Lett.* **62**, 1259 (1989).
- [18] P. B. Corkum, Plasma perspective on strong field multiphoton ionization, *Phys. Rev. Lett.* **71**, 1994 (1993).
- [19] J.-M. Rost, Semiclassical S-matrix theory for atomic fragmentation, *Physics Reports* **297**, 271 (1998).
- [20] G. van de Sand and J. M. Rost, Semiclassical description of multiphoton processes, *Phys. Rev. A* **62**, 053403 (2000).
- [21] J. Liu, Classical trajectory perspective of atomic ionization in strong laser fields: semiclassical modeling (Springer Science & Business Media, 2013).
- [22] M. Lewenstein, K. C. Kulander, K. J. Schafer, and P. H. Bucksbaum, Rings in above-threshold ionization: A quasiclassical analysis, *Phys. Rev. A* **51**, 1495 (1995).
- [23] T.-M. Yan and D. Bauer, Sub-barrier Coulomb effects on the interference pattern in tunneling-ionization photoelectron spectra, *Phys. Rev. A* **86**, 053403 (2012).
- [24] M. Li, X. Sun, X. Xie, Y. Shao, Y. Deng, C. Wu, Q. Gong, and Y. Liu, Revealing backward rescattering photoelectron interference of molecules in strong infrared laser fields, *Scientific reports* **5**, 1 (2015).
- [25] S. Brennecke and M. Lein, Strong-field photoelectron holography beyond the electric dipole approximation: A semiclassical analysis, *Phys. Rev. A* **100**, 023413 (2019).
- [26] S. D. López and D. G. Arbó, Holographic interference in atomic photoionization from a semiclassical standpoint, *Phys. Rev. A* **100**, 023419 (2019).
- [27] D. Bauer and P. Koval, Qprop: A Schrödinger-solver for intense laser-atom interaction, *Computer Physics Communications* **174**, 396 (2006).
- [28] Q. Li, X.-M. Tong, T. Morishita, H. Wei, and C. D. Lin, Fine structures in the intensity dependence of excitation and ionization probabilities of hydrogen atoms in intense 800-nm laser pulses, *Phys. Rev. A* **89**, 023421 (2014).
- [29] L. V. Keldysh et al., Diagram technique for nonequilibrium processes, *Sov. Phys. JETP* **20**, 1018 (1965).
- [30] F. H. M. Faisal, Multiple absorption of laser photons by atoms, *Journal of Physics B: Atomic and Molecular Physics* **6**, L89 (1973).
- [31] H. R. Reiss, Effect of an intense electromagnetic field on a weakly bound system, *Phys. Rev. A* **22**, 1786 (1980).
- [32] S. Popruzhenko and D. Bauer, Strong field approximation for systems with Coulomb interaction, *Journal of Modern Optics* **55**, 2573 (2008).
- [33] S. V. Popruzhenko, G. G. Paulus, and D. Bauer, Coulomb-corrected quantum trajectories in strong-field ionization, *Phys. Rev. A* **77**, 053409 (2008).
- [34] T.-M. Yan, S. V. Popruzhenko, M. J. J. Vrakking, and D. Bauer, Low-Energy Structures in Strong Field Ionization Revealed by Quantum Orbits, *Phys. Rev. Lett.* **105**, 253002 (2010).
- [35] L. G. Gouy, Sur une propriété nouvelle des ondes lumineuses (Gauthier-Villars, 1890).
- [36] M. C. Gutzwiller, Chaos in classical and quantum mechanics, Vol. 1 (Springer Science & Business Media, 2013).
- [37] S. Brennecke, N. Eicke, and M. Lein, Gouy's Phase Anomaly in Electron Waves Produced by Strong-Field Ionization, *Phys. Rev. Lett.* **124**, 153202 (2020).



- [38] P. Sikiwie, Caustic ring singularity, *Phys. Rev. D* **60**, 063501 (1999).
- [39] H. M. Nussenzveig, *Diffraction effects in semiclassical scattering*, Vol. 1 (Cambridge University Press, 2006).
- [40] Q. Z. Xia, J. F. Tao, J. Cai, L. B. Fu, and J. Liu, Quantum Interference of Glory Rescattering in Strong-Field Atomic Ionization, *Phys. Rev. Lett.* **121**, 143201 (2018).
- [41] M. V. Berry, Uniform approximation: a new concept in wave theory, *Science Progress (1933- )* **57**, 43 (1969).
- [42] M. V. Berry, Uniform approximations for glory scattering and diffraction peaks, *Journal of Physics B: Atomic and Molecular Physics* **2**, 381 (1969).
- [43] F. J. Dyson, The *S* Matrix in Quantum Electrodynamics, *Phys. Rev.* **75**, 1736 (1949).
- [44] M. C. Gutzwiller, Phase-Integral Approximation in Momentum Space and the Bound States of an Atom, *Journal of mathematical Physics* **8**, 1979 (1967).
- [45] M. V. Berry, Nature's optics and our understanding of light, *Contemporary Physics* **56**, 2 (2015).
- [46] K. W. Ford and J. A. Wheeler, Semiclassical description of scattering, *Annals of Physics* **7**, 259 (1959).
- [47] J. A. Adam, The mathematical physics of rainbows and glories, *Physics Reports* **356**, 229 (2002).
- [48] D. B. Milošević, G. G. Paulus, D. Bauer, and W. Becker, Above-threshold ionization by few-cycle pulses, *Journal of Physics B: Atomic, Molecular and Optical Physics* **39**, R203 (2006).
- [49] M. Li, J.-W. Geng, M. Han, M.-M. Liu, L.-Y. Peng, Q. Gong, and Y. Liu, Subcycle nonadiabatic strong-field tunneling ionization, *Phys. Rev. A* **93**, 013402 (2016).
- [50] D. D. Morrison, J. D. Riley, and J. F. Zaccanaro, Multiple shooting method for two-point boundary value problems, *Communications of the ACM* **5**, 613 (1962).
- [51] N. I. Shvetsov-Shilovski, M. Lein, L. B. Madsen, E. Räsänen, C. Lemell, J. Burgdörfer, D. G. Arbó, and K. Tökési, Semiclassical two-step model for strong-field ionization, *Phys. Rev. A* **94**, 013415 (2016).
- [52] K. Möhring, S. Levit, and U. Smilansky, On the semiclassical green's function in the energy-representation, *Annals of Physics* **127**, 198 (1980).
- [53] M. L. Du and J. Delos, Effect of closed classical orbits on quantum spectra: ionization of atoms in a magnetic field, *Phys. Rev. Lett.* **58**, 1731 (1987).
- [54] V. P. Maslov and M. V. Fedoriuk, *Semi-classical approximation in quantum mechanics*, Vol. 7 (Springer Science & Business Media, 2001).
- [55] J. B. Delos, Semiclassical Calculation of Quantum Mechanical Wave Functions. *Advances in Chemical Physics*, **132**, 161 (2009).
- [56] X.-M. Tong and S.-I. Chu, Theoretical study of multiple high-order harmonic generation by intense ultrashort pulsed laser fields: A new generalized pseudospectral time-dependent method, *Chemical Physics*, **217**, 119 (1997).